

# Effect of Groove Size on Aerodynamic Performance of a Low Reynolds Number UAV Propeller

Aravind SEENI\*

\*Corresponding author

International Institute for Aerospace Engineering and Management,  
Jain (Deemed-to-be University), 562112 Bangalore, India,  
s.aravind@jainuniversity.ac.in

DOI: 10.13111/2066-8201.2022.14.1.14

Received: 17 August 2021/ Accepted: 09 November 2021/ Published: March 2022

Copyright © 2022. Published by INCAS. This is an “open access” article under the CC BY-NC-ND license (<http://creativecommons.org/licenses/by-nc-nd/4.0/>)

**Abstract:** *Small-scale propellers typically have low aerodynamic efficiency. Improving the aerodynamic performance and efficiency of these propellers will enhance the endurance and operational range of UAVs. The desired requirement is a propeller design that can produce improved thrust and reduced torque. In order to fulfil such an objective, a novel technique known as the grooved design is studied on a small-scale propeller. Numerical investigations are performed on Applied Precision Composites 10×7 Slow Flyer propeller. Computational Fluid Dynamics is used to analyze this novel design. The grooved cross-sections considered have a rectangular geometry measuring 0.1×0.1mm and 0.1×0.2mm which are placed at 0.09c, 0.17c, 0.32c and 0.42c from the leading edge. The results of the study showed that the presence of grooves had modified the flow characteristics only to detrimentally impact the thrust performance. However, the grooves improved power performance due to torque reduction. The analysis of the  $K_F$  results showed, in most models, the low torque relative to the baseline in the operational range of the low to medium advance ratio range. The improvement in torque, however, did not improve efficiency in all models.*

**Key Words:** *passive flow control, grooved propeller, aerodynamic performance, UAV range, UAV endurance*

## 1. INTRODUCTION

UAVs, also referred to as drones, have been widely used in many scientific applications of remote sensing. Examples of such applications are archaeology [1], atmospheric research [2], disaster prevention and recovery [3], ecology [4] and education [5]. UAVs are also known to be useful in next-generation applications such as product delivery from business source to end-user. These UAVs usually weigh between 1 and 10kg and are driven by propellers operating at a low Reynolds number (Re) [6]. The operational Re range for small UAVs is between 1000 and 10000. Improving the efficiency of these small UAV propellers helps to improve the endurance of UAVs and thus the operational range. Research on improving the efficiency of UAV propellers helps to increase and add value to this important future application. The desired requirement is a propelling device capable of producing improved thrust and reduced torque at a low Re. Modern research is concerned with improving the thrust through flow modifiers or flow control technique. These flow modifiers alter the fluid flow such that the flow trajectory is optimized around the aerodynamic body to attain the desired performance. This research deals with the application of passive flow control technique known as the

grooved design on an arbitrary propeller. Flow control means the control of the flow separation in a fluid medium from a surface through different techniques. Flow control techniques have been implemented for different surfaces and bodies. For a bluff body, a variety of flow control techniques were studied in the past [7]. Similarly, the flow control was also studied in aerodynamic bodies. Amitay *et al.* [8] studied the use of synthetic jets using experimental methods for an airfoil. Corke *et al.* [9] reviewed the use of Single Dielectric Barrier Discharge plasma actuators on an airfoil. Huang *et al.* [10] studied the use of single dielectric barrier discharge plasma actuators on the turbine blade cascade. Bons *et al.* [11] studied the concept of pulsed vortex generator jets on the surface of a low-pressure turbine blade. Nishri and Wygnanski [12] studied the effects of the periodic excitation or perturbations on promoting and delaying reattachment of initially separated flow for a flap. Seifert and Pack [13] studied the active flow control on a wall-mounted hump at a high  $Re$  which simulated the flow over an airfoil at zero incidence. Greenblatt and Wygnanski [14] investigated the effect of the periodic excitation on a NACA0015 airfoil undergoing pitch oscillations. You and Moin [15] also studied the use of synthetic jets on an airfoil. Little *et al.* [10] investigated the separation control on a high-lift airfoil using a single dielectric barrier discharge plasma actuator.

The current research is concerned with studying the flow control technique called grooved design. In the present study, a comprehensive study on grooved propeller design has been performed with the aim to study its significance for aeronautical application. The unique features of an aeronautical propeller are low torque, high thrust and high efficiency during operation. The effect of the variation in groove size on the performance characteristics of the propeller will be investigated. Till now, no studies have considered the effect of geometrical variation of grooves on aerodynamic performance. The size variation of grooves could have either favorable or detrimental impact on the aerodynamic performance. These have not been investigated so far and will be investigated in the current work.

## 2. METHODOLOGY

The study of the fluid flow on an arbitrary body in modern research can be successfully performed by solving governing equations of fluid flow. The equations are called the Navier-Stokes equations. The CFD method, which uses numerical approaches, is used to solve these equations. For the present research, RANS simulations are preferred over Large Eddy Simulation (LES) and Direct Numerical Simulation (DNS). The use of DNS may provide highly accurate solutions than RANS, but it requires prohibitively a CPU of high performance which withstands high computational loads. Similarly, LES lies in between RANS and DNS in terms of computational cost and numerical accuracy. As a first step of initiating the research on fluid dynamic analysis of grooved propeller, RANS is preferred over other methods.

### 2.1 Baseline propeller description

*Applied Precision Composites (APC) 10×7 Slow Flyer (SF)* is considered as the baseline propeller in this study. APC10x7SF is widely used in low  $Re$  applications such as small-scale UAVs. This propeller is chosen based on the availability of data from the experiments of Brandt *et al.* [16]. The propeller has a diameter ( $D$ ) of 0.254 m and pitch of 0.1778 m. Low  $Re$  Eppler E63 air foil sections near the hub and thin Clark-Y air foil sections near the tip are used to design the propeller. For the simulation, the propeller is assumed to be rotating at a constant rotational speed of 3008rpm. The fluid assumed for the simulation is air which is considered to be steady and the flow is viscous and incompressible. The fluid properties of air are assumed with  $\rho$  of 1.225kg/m<sup>3</sup> and  $\mu$  of 1.7894×10<sup>-5</sup>kgm<sup>-1</sup>s<sup>-1</sup>.

## 2.2 CAD modelling

The design of propellers is performed using CAD software Catia v5. For the design of grooved propeller, baseline propeller model is modified with grooves of varying dimensions. To study the effect of groove geometry, grooves are placed at specific positions from the leading edge at  $0.09c$ ,  $0.17c$ ,  $0.32c$  and  $0.42c$  distance. The positions are further illustrated in Fig. 1 and Fig. 2. The dimensions of the grooves are varied for different positions, as listed in Table 1. The position of grooves,  $0.09c$ ,  $0.17c$ ,  $0.32c$  and  $0.42c$  are selected by dividing the chord length of air foil into six equal divisions. The first four divisions,  $0.09c$ ,  $0.17c$ ,  $0.32c$  and  $0.42c$  are selected based design feasibility existing for maximum groove depth of  $0.3\text{mm}$ . The other two chord length positions are not feasible for maximum groove depth considered in this research and therefore not included.

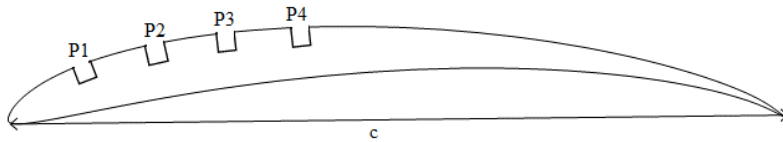


Fig. 1 – Illustration of grooved APC10x7SF propeller cross-section with groove at positions, P1 ( $0.09c$ ), P2 ( $0.17c$ ), P3 ( $0.32c$ ) and P4 ( $0.42c$ )

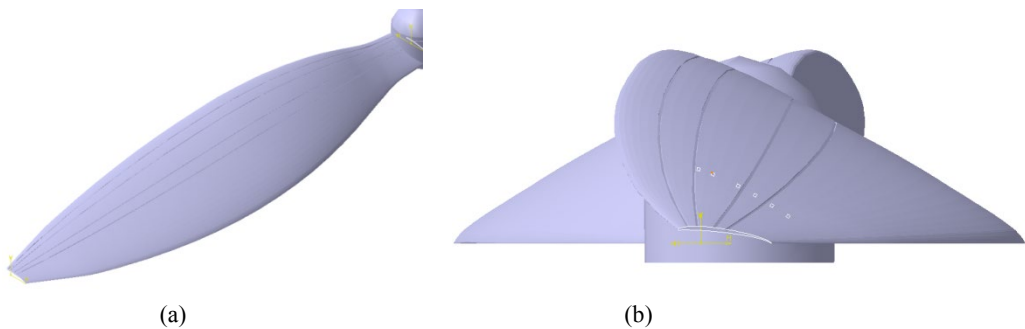


Fig. 2 – Illustration of propeller with grooves of dimensions  $0.1\text{mm} \times 0.2\text{mm}$  positioned at  $0.09c$ ,  $0.17c$ ,  $0.32c$  and  $0.42c$  (a) isometric view of blade (b) front view of propeller

Table 1. – Propeller configurations to study the effect of groove geometry

Name	Groove size	Groove position, $x_{LE}$
Model – 1	$0.1\text{mm} \times 0.1\text{mm}$	$0.09c$
Model – 2	$0.1\text{mm} \times 0.1\text{mm}$	$0.32c$
Model – 3	$0.1\text{mm} \times 0.1\text{mm}$	$0.42c$
Model – 4	$0.1\text{mm} \times 0.2\text{mm}$	$0.09c$
Model – 5	$0.1\text{mm} \times 0.2\text{mm}$	$0.17c$
Model – 6	$0.1\text{mm} \times 0.2\text{mm}$	$0.32c$
Model – 7	$0.1\text{mm} \times 0.2\text{mm}$	$0.42c$

## 2.3 Computational Fluid Dynamics

### 2.3.1 Computational domain

The computational domain consists of a 3D computational grid. A Multiple Reference Frame (MRF) approach is implemented to model the computational domain. Two reference frames comprising one stationary and one rotational frame are assumed. The propeller is enclosed within the rotational reference frame which rotates at a speed of  $3008\text{rpm}$ . The rotational

reference frame is designed with a cylindrical geometry having a diameter of  $1.1D$ . The stationary reference frame is a cubic enclosure and designed with a constant side length of  $8D$ .

### 2.3.2 Mesh

The domain is meshed into multiple numbers of small fluid control volumes in which the velocity components  $u$ ,  $v$  and  $w$  and pressure component  $p$  at the centre of all the control volumes are solved. An unstructured mesh consisting of tetrahedron elements is used. It is known that while the structured mesh is used for its refinement, the use of unstructured mesh does not deteriorate the quality of results with respect to numerical accuracy [17]–[19]. The mesh for the grooved designs is performed with identical grid sizes of the baseline propeller. The meshes in the groove locations are maintained at sufficient mesh density in order to accurately capture the flow characteristics. Grid on a propeller with two grooves as an example for illustration purpose is provided in Fig. 3.

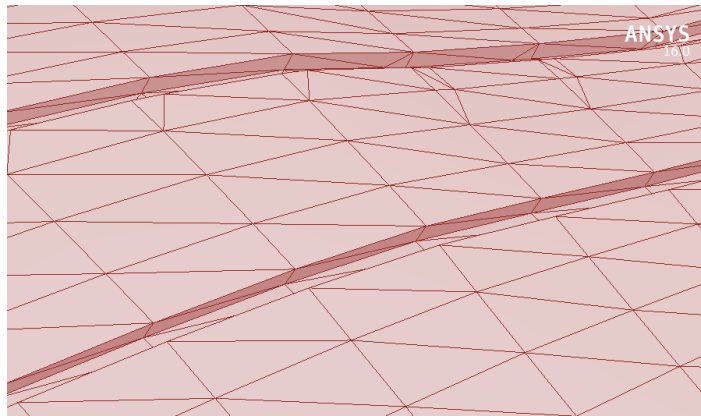


Fig. 3 – Illustration of grid around 3D groove on the propeller

### 2.3.3 Boundary conditions and settings

At the wall, which is the rotating domain, a no slip condition is assumed. Inlet fluid velocities ranging between  $2.4384\text{m/s}$  and  $10.1473\text{m/s}$  for corresponding  $J$  conditions between  $0.192$  and  $0.799$  are assumed. For pressure-velocity coupling, Semi-Implicit Method for Pressure-Linked Equations (SIMPLE) scheme is assumed. The gradients are assigned with Least-Squares Cell-based algorithm. The standard scheme of interpolation is assigned for pressure. For Turbulent Dissipation Rate, Turbulent Kinetic Energy and momentum, a second order upwind interpolation scheme is applied. The fluid is assumed to be air with the following properties:  $T=25^\circ\text{C}$ ,  $\rho=1.225\text{kg/m}^3$  and  $\mu=1.7894\times 10^{-5}\text{kgm}^{-1}\text{s}^{-1}$ . The one-equation Spalart-Allmaras (S-A) model will provide turbulence closure. The S-A model is selected based on its application in aerodynamic flows.

### 2.4 Expressions for aerodynamic coefficients of a propeller

The coefficients representing the aerodynamic performance of propeller are provided. The thrust coefficient can be expressed as in Eqn. 1.

$$K_T = \frac{T}{\rho n^2 D^4} \quad (1)$$

where  $T$  is the thrust force,  $\rho$  is the fluid density,  $n$  is the rotational speed, and  $D$  is the diameter. The torque coefficient can be expressed as in Eqn. 2.

$$K_Q = \frac{Q}{\rho n^2 D^5} \quad (2)$$

where  $Q$  is the torque. The power coefficient can be expressed as in Eqn. 3.

$$K_P = \frac{P}{\rho n^3 D^5} \quad (3)$$

where  $P$  is power.  $P$  is estimated from torque  $Q$  and propeller speed as in Eqn. 4:

$$P = 2\pi nQ \quad (4)$$

The efficiency is a function of  $K_T$ ,  $K_P$  and  $J$  and can be expressed as in Eqn. 5. Also, it can be expressed as per Eqn. 6.

$$\eta = J \frac{K_T}{K_P} \quad (5)$$

$$\eta = \frac{J}{2\pi} \frac{K_T}{K_Q} \quad (6)$$

For the propeller case, the errors are estimated again by comparing CFD obtained numerical results with experimental data. The percentage difference in error for various performance coefficients between numerical and experimental results will be estimated using the expressions as given in Eqns. 7-9.

$$\Delta K_T(\%) = \frac{K_{T,CFD} - K_{T,EXP}}{K_{T,EXP}} \times 100 \quad (7)$$

$$\Delta K_P(\%) = \frac{K_{P,CFD} - K_{P,EXP}}{K_{P,EXP}} \times 100 \quad (8)$$

$$\Delta \eta(\%) = \frac{\eta_{CFD} - \eta_{EXP}}{\eta_{EXP}} \times 100 \quad (9)$$

where  $K_{T,EXP}$  refers to experimental  $K_T$  of baseline design,  $K_{T,CFD}$  refers to numerical  $K_T$  of grooved design,  $K_{P,EXP}$  refers to experimental  $K_P$  of baseline design,  $K_{P,CFD}$  refers to numerical  $K_P$  of grooved design,  $\eta_{EXP}$  refers to experimental  $\eta$  of baseline design,  $\eta_{CFD}$  refers to numerical  $\eta$  of grooved design.

### 3. RESULTS AND DISCUSSIONS

#### 3.1 Verification

Grid independency tests are performed for numerical verification of results. The grid resolution method is used to perform this test.

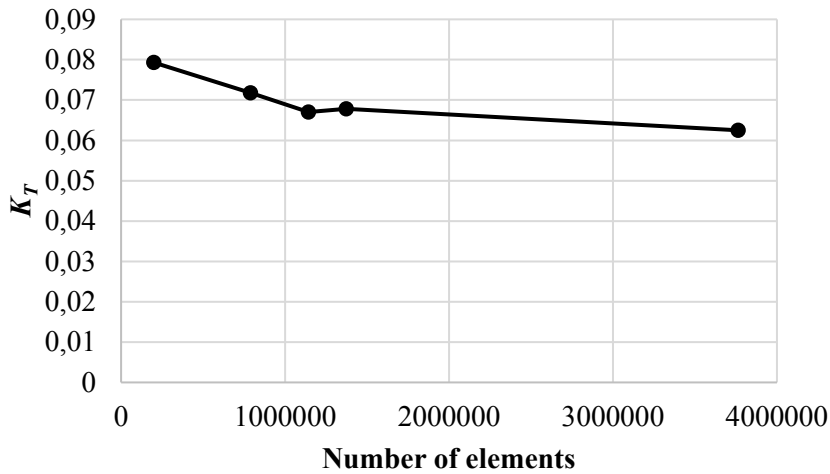
Five grids of increasing mesh resolution as detailed in Table 2 are used to simulate propeller rotation at 3008 rpm. In the grid resolution method, the lowest difference in error with improvement in grid resolution is utilized.

This test requires performing the procedures of establishing mesh independency for a single  $J$  condition. Therefore, this test will be performed for  $J$  condition of 0.486. The results are provided in Table 2.

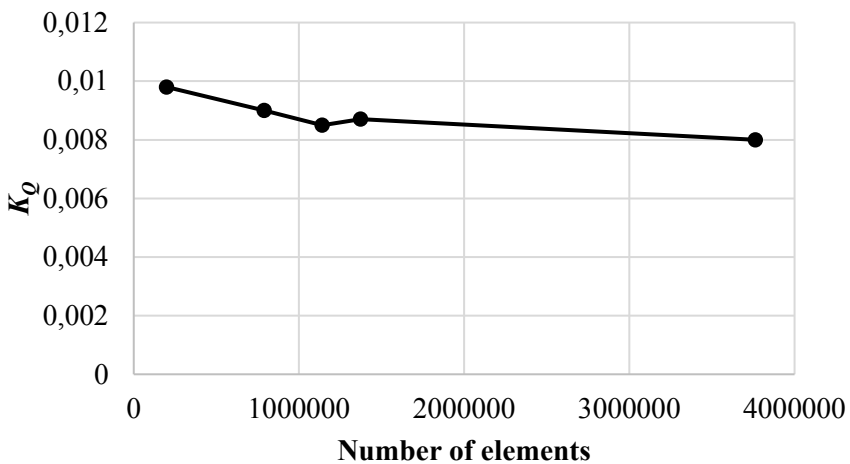
Table 2. – Grid independence test results for baseline propeller performance assuming condition  $J=0.486$

Grid	Refinement	$K_T$	$K_Q$	$10K_P$
Grid 1	Coarsest	0.0793	0.0098	0.6132
Grid 2	Coarse	0.0718	0.0090	0.5655
Grid 3	Medium	0.0670	0.0085	0.53457
Grid 4	Mid-fine	0.0678	0.0087	0.5440
Grid 5	Fine	0.0625	0.0080	0.5033

As it can be seen in Table 2(a), for  $K_T$ , Table 2(b) for  $K_Q$ , the values show a minimal change when the resolution improves from medium (Grid 3) to fine (Grid 4). The smallest difference in error can be observed only for this grid resolution change. The medium mesh provides the necessary convergence requirement at lowest cost. The medium mesh, therefore, provides the necessary convergence in this study.



(a)



(b)

Fig. 4 – Grid independence results for baseline propeller performance assuming condition  $J=0.486$

(a)  $K_T$  and (b)  $K_Q$

### 3.2 Validation

The experimental data for the baseline APC10x7SFpropeller considered is obtained from an online academic database of propeller performance data maintained by Brandt *et al.* [16]. The database provides experimental data for the chosen propeller with the fluid assumed to be air and operational speed of 3008 rpm.

Table 3. – Validation of thrust performance of baseline APC10x7SF propeller

Case	$J$	$T_{EXP}$ [N]	$K_{T,EXP}$	$T_{CFD}$ [N]	$K_{T,CFD}$	$\Delta K_T$ [%]
1	0.192	1.6109	0.1257	1.4927	0.1165	-7.3
2	0.236	1.5135	0.1181	1.4421	0.1125	-4.7
3	0.282	1.4212	0.1109	1.3804	0.1077	-2.9
4	0.334	1.3161	0.1027	1.3020	0.1016	-1.1
5	0.383	1.2174	0.0950	1.2198	0.0952	0.2
6	0.432	1.1085	0.0865	1.1290	0.0881	1.8
7	0.486	0.9816	0.0766	1.0172	0.0794	3.6
8	0.527	0.8868	0.0692	0.9257	0.0722	4.4
9	0.573	0.7779	0.0607	0.8163	0.0637	4.9
10	0.628	0.6318	0.0493	0.6707	0.0523	6.2
11	0.659	0.5459	0.0426	0.5846	0.0456	7.1
12	0.717	0.3716	0.0290	0.4172	0.0326	12.3
13	0.773	0.1833	0.0143	0.2441	0.0190	33.2
14	0.799	0.1000	0.0078	0.1575	0.0123	57.6

Table 4. – Validation of power performance of baseline APC10x7SF propeller

Case	$J$	$P_{EXP}$ [W]	$10K_{P,EXP}$	$P_{CFD}$ [W]	$10K_{P,CFD}$	$\Delta K_P$ [%]
1	0.192	0.0681	0.6810	11.2092	0.6869	0.9
2	0.236	0.0662	0.6620	11.1833	0.6853	3.5
3	0.282	0.0646	0.6460	11.0964	0.6800	5.3
4	0.334	0.0629	0.6290	10.9384	0.6703	6.6
5	0.383	0.0610	0.6100	10.7279	0.6574	7.8
6	0.432	0.0586	0.5860	10.4444	0.6400	9.2
7	0.486	0.0553	0.5530	10.0309	0.6147	11.2
8	0.527	0.0526	0.5260	9.6431	0.5909	12.3
9	0.573	0.0492	0.4920	9.1313	0.5596	13.7
10	0.628	0.0444	0.4440	8.3878	0.5140	15.8
11	0.659	0.0417	0.4170	7.9303	0.4860	16.5
12	0.717	0.0355	0.3550	6.9573	0.4263	20.1
13	0.773	0.0283	0.2830	5.9129	0.3623	28.0
14	0.799	0.0252	0.2520	5.3987	0.3308	31.3

Table 5. – Validation of  $\eta$  of baseline APC10x7SF propeller

Case	$J$	$\eta_{EXP}$	$\eta_{CFD}$	$\Delta\eta$ [%]
1	0.192	0.3550	0.3256	-8.3
2	0.236	0.4210	0.3875	-8.0
3	0.282	0.4840	0.4467	-7.7
4	0.334	0.5460	0.5063	-7.3
5	0.383	0.5960	0.5545	-7.0
6	0.432	0.6390	0.5946	-6.9
7	0.486	0.6740	0.6276	-6.9
8	0.527	0.6940	0.6442	-7.2
9	0.573	0.7080	0.6523	-7.9
10	0.628	0.6970	0.6395	-8.3
11	0.659	0.6740	0.6186	-8.2
12	0.717	0.5860	0.5475	-6.6
13	0.773	0.3910	0.4063	3.9
14	0.799	0.2470	0.2968	20.2

The comparison of CFD and experimentally obtained results are provided in tabular form. Table 3 provides the results of  $K_T$ . The error for the various cases is obtained within acceptable limits for most  $J$  in the lower range between 0.192 and 0.717. For two high  $J$  cases, the error exceeds the limits. Table 4 provides comparative results of  $K_P$ . For this coefficient, CFD predicted values within acceptable error limits for nine  $J$  cases. For five cases of higher  $J$ , the error deviations are higher than 15%. Table 5 provides comparative results of  $\eta$ . The errors for the  $\eta$  are very close to experimental results for most  $J$  except for  $J=0.799$ .

### 3.3 Effect of groove size on propeller performance

#### 3.3.1 Model – 1

The performance and efficiency results of Model – 1 grooved design are provided in Table 6.

Table 6. – Performance and efficiency results of Model – 1

Case	Condition	$K_T$	$\Delta K_T$ [%]	$10K_P$	$\Delta K_P$ [%]	$\eta$ [%]	$\Delta\eta$ [%]
	$J$						
1	0.192	0.1089	-13.38	0.6386	-6.22	32.74	-7.79
2	0.236	0.1049	-11.16	0.6313	-4.64	39.22	-6.83
3	0.282	0.0998	-10.03	0.6212	-3.84	45.30	-6.41
4	0.334	0.0942	-8.26	0.6104	-2.96	51.56	-5.57
5	0.383	0.0874	-8.02	0.5935	-2.71	56.39	-5.39
6	0.432	0.0805	-6.93	0.5738	-2.08	60.61	-5.15
7	0.486	0.0714	-6.78	0.5461	-1.24	63.54	-5.72
8	0.527	0.0648	-6.30	0.5233	-0.52	65.30	-5.90
9	0.573	0.0566	-6.79	0.4927	0.14	65.80	-7.06
10	0.628	0.0459	-6.86	0.4517	1.74	63.83	-8.42
11	0.659	0.0396	-7.00	0.4250	1.91	61.43	-8.85
12	0.717	0.0275	-5.21	0.3735	5.20	52.78	-9.94
13	0.773	0.0148	3.64	0.3190	12.73	35.91	-8.16
14	0.799	0.0094	20.81	0.2938	16.59	25.63	3.75

Model – 1 grooved design has reduced  $K_T$  compared to unmodified baseline for  $J$  from 0.192 to 0.717.

The decrement varies between  $-5.21\%$  to  $-13.38\%$  for the aforementioned  $J$  range. An improvement in  $K_T$  is observed for  $J$  cases 13 and 14.  $K_P$  is found to be reduced for  $J$  between 0.192 to 0.527.

From  $J$  of 0.573, the  $K_P$  increases. The increase is found to be in the range between 0.14% and 16.59%. The  $\eta$  was found to be decreased for  $J$  from 0.192 to 0.773. The decrement ranges between  $-5.15\%$  and  $-9.94\%$ . Only for  $J$  of 0.799, the  $\eta$  was found to be increased.

The physics of the fluid flow around a propeller designed with a groove can be explained in this way.

A propeller is a body with three-dimensional geometry with a twist. The twist (or geometric twist) is incorporated along the radial direction such that the angle of attack varies along the blade span.

The twist serves the purpose of maintaining a particular lift (or thrust) distribution along the span. In the case of APC10x7SF propeller, the blades also incorporate aerodynamic twist, in addition, in which both Eppler E63 and Clark-Y air foils are used at different sections along the span. The presence of air foil sections incorporating twist, during rotation of the propeller causes the fluid to accelerate around it.

The velocity of fluid due to the acceleration is three-dimensional and the components can be resolved in all three dimensions.

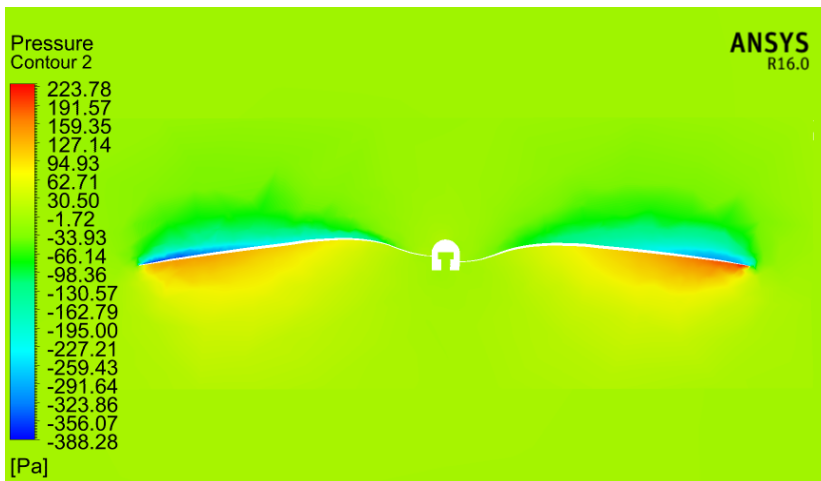
The velocity changes are more pronounced near the vicinity of the rotating propeller in the fore and aft.

As the distance in the aft of the propeller increases, the disturbance to the flow deteriorates and the velocity reduces to zero after dissipation of wake. The end-result is the production of thrust force and torque moment.

The desirable design characteristics of a propeller is its ability to develop high thrust and low torque.

The introduction of 3D groove at 0.09c (Model – 1) causes the fluid to accelerate at reduced speed compared to baseline.

The velocity is reduced in the stream wise direction and the three-dimensional velocity distribution around the groove modified. This results in loss of fluid acceleration thus inherently reducing thrust.



(a)

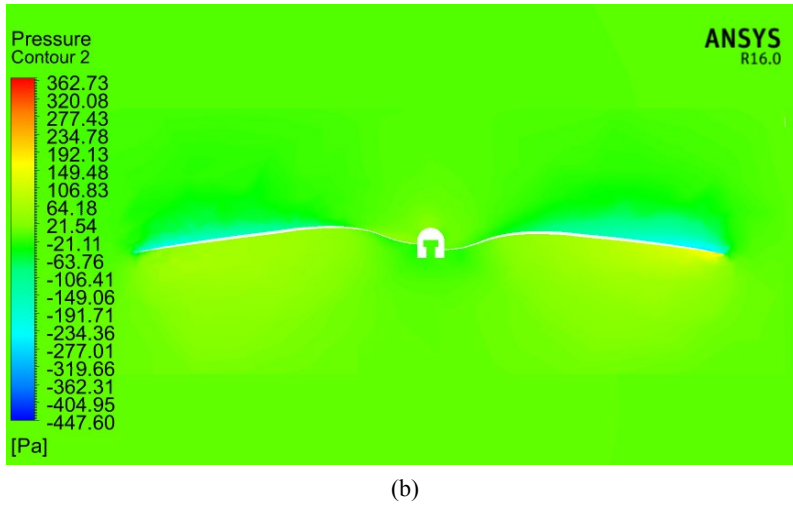


Fig. 5 – Pressure contour of flow around Model – 1 propeller for (a)  $J=0.334$  and (b)  $J=0.573$

Also the pressure field is modified in the fore and aft. This is illustrated in Fig. 5 for two  $J$  cases, 0.334 and 0.573. Lower peak pressures are maintained at the pressure side (aft) as compared to baseline whereas lower low pressures are maintained at the suction side (fore) as compared to baseline for  $J=0.334$ . For  $J=0.573$ , lower peak pressures are maintained at the pressure side (aft) as compared to baseline whereas higher low pressures are maintained at the suction side (fore) as compared to baseline. The modified pressure levels on the pressure side and on the suction side in the presence of groove for two  $J$  cases, 0.334 and 0.573 can be viewed along the  $yz$  plane bisecting the flow field. The decomposition of velocity in the radial ( $u$ - component), rotational ( $v$ - component) and axial ( $w$ - component) directions are presented in Fig. 6 for  $J=0.334$  and in Fig. 7 for  $J=0.573$ . During rotation, the fluid velocity is modified when traversing between leading edge and trailing edge and when traversing the groove. For Model – 1, the radial velocity component is reduced, rotational velocity component is reduced and axial velocity component is increased compared to baseline for  $J=0.334$ . The radial velocity component is increased, rotational velocity component is reduced and axial velocity component is increased compared to baseline for  $J=0.573$  for this model.

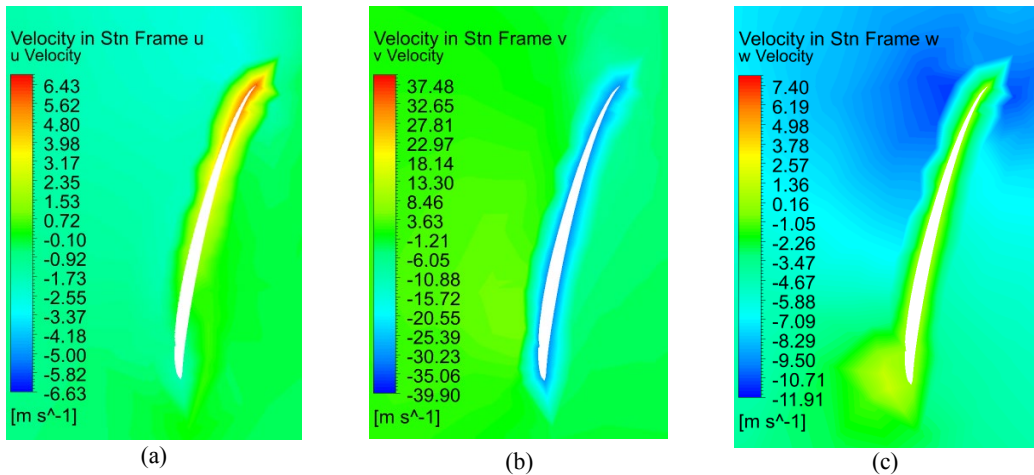


Fig. 6 – Velocity contour of flow around Model – 1 propeller at 0.75R radial distance for  $J=0.334$   
 (a) radial component (b) rotational component (c) axial component

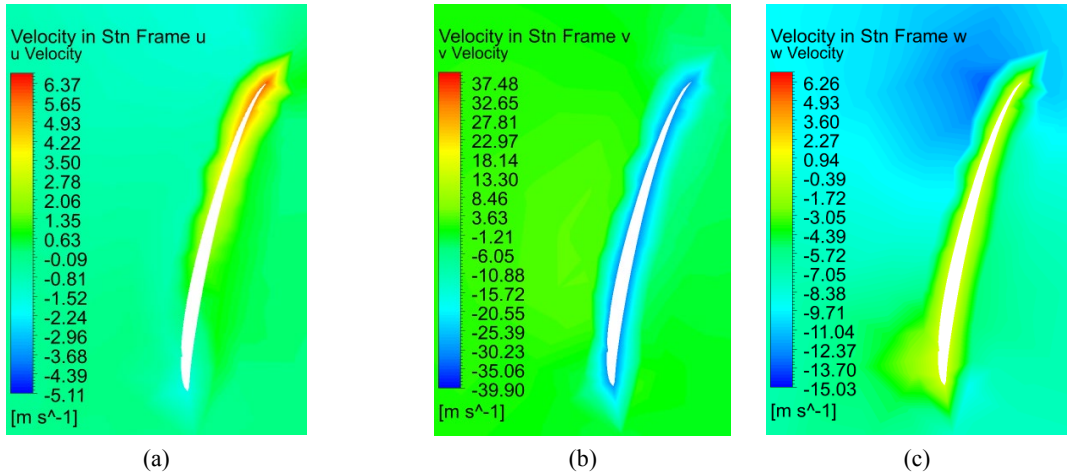


Fig. 7 – Velocity contour of flow around Model – 1 propeller at 0.75R radial distance for  $J=0.573$   
 (a) radial component (b) rotational component (c) axial component

### 3.3.2 Model – 2

The performance and efficiency results of Model – 2 grooved design are provided in Table 7. The relative difference between the results with baseline propeller is also listed in the table.

Table 7. – Performance and efficiency results of Model – 2

Case	Condition	$K_T$	$\Delta K_T$ [%]	$10K_P$	$\Delta K_P$ [%]	$\eta$ [%]	$\Delta\eta$ [%]
	$J$						
1	0.192	0.1089	-13.33	0.6364	-6.55	32.87	-7.41
2	0.236	0.1049	-11.14	0.6290	-4.98	39.37	-6.47
3	0.282	0.1005	-9.34	0.6228	-3.59	45.52	-5.95
4	0.334	0.0941	-8.42	0.6084	-3.27	51.63	-5.44
5	0.383	0.0876	-7.74	0.5937	-2.68	56.54	-5.13
6	0.432	0.0808	-6.65	0.5726	-2.30	60.93	-4.65
7	0.486	0.0723	-5.65	0.5471	-1.08	64.21	-4.74
8	0.527	0.0650	-6.12	0.5213	-0.89	65.68	-5.37
9	0.573	0.0564	-7.16	0.4903	-0.35	65.86	-6.98
10	0.628	0.0459	-6.89	0.4503	1.41	64.02	-8.15
11	0.659	0.0401	-5.97	0.4255	2.03	62.04	-7.95
12	0.717	0.0282	-2.85	0.3760	5.90	53.73	-8.31
13	0.773	0.0158	10.23	0.3225	13.94	37.79	-3.36
14	0.799	0.0097	24.15	0.2952	17.15	26.21	6.11

Model – 2 grooved design performance results exhibit reduced  $K_T$  ranging from -2.85% to -13.33%. For  $J$  0.773 and 0.799,  $K_T$  increased with respect to the baseline.  $K_P$  was found to be decreased for  $J$  between 0.192 and 0.573.

For  $J$  from 0.628 to 0.799, the  $K_P$  increased. The  $\eta$  was found to be decreased for all  $J$  except 0.799. For 0.799  $J$ , the  $\eta$  increased by 6.11%.

### 3.3.3 Model – 3

The performance and efficiency results of Model – 3 grooved design are provided in Table 8. The relative difference between the results with baseline propeller is also listed in the table.

Table 8. – Performance and efficiency results of Model – 3

Case	Condition	$K_T$	$\Delta K_T$ [%]	$10K_P$	$\Delta K_P$ [%]	$\eta$ [%]	$\Delta \eta$ [%]
	$J$						
1	0.192	0.1076	-14.39	0.6324	-7.14	32.67	-7.96
2	0.236	0.1029	-12.91	0.6235	-5.82	38.93	-7.53
3	0.282	0.0979	-11.76	0.6128	-5.14	45.03	-6.95
4	0.334	0.0918	-10.58	0.5994	-4.71	51.17	-6.28
5	0.383	0.0853	-10.17	0.5841	-4.24	55.95	-6.12
6	0.432	0.0782	-9.58	0.5635	-3.84	59.96	-6.16
7	0.486	0.0695	-9.28	0.5338	-3.48	63.28	-6.12
8	0.527	0.0629	-9.04	0.5125	-2.56	64.72	-6.75
9	0.573	0.0549	-9.57	0.4822	-1.99	65.23	-7.87
10	0.628	0.0448	-9.17	0.4435	-0.11	63.40	-9.03
11	0.659	0.0387	-9.22	0.4195	0.59	60.76	-9.86
12	0.717	0.0268	-7.53	0.3709	4.47	51.84	-11.54
13	0.773	0.0147	2.53	0.3190	12.71	35.53	-9.13
14	0.799	0.0089	14.67	0.2927	16.16	24.41	-1.17

Model – 3 grooved design performance results show that  $K_T$  decreased for  $J$  of 0.192 to 0.717. For  $J$  of 0.773 to 0.799,  $K_T$  increased.  $K_P$  decreased relative to baseline for  $J$  of 0.192 to 0.628. For  $J$  of 0.659 to 0.799, the  $K_P$  increased. The  $\eta$  was found to be decreased for all  $J$  relative to baseline.

### 3.3.4 Model – 4

The performance and efficiency results of Model – 4 grooved design are provided in Table 9. The relative difference between the results with baseline propeller is also listed in the table.

Table 9. – Performance and efficiency results of Model – 4

Case	Condition	$K_T$	$\Delta K_T$ [%]	$10K_P$	$\Delta K_P$ [%]	$\eta$ [%]	$\Delta \eta$ [%]
	$J$						
1	0.192	0.1081	-14.01	0.6309	-7.36	32.89	-7.34
2	0.236	0.1041	-11.84	0.6255	-5.52	39.28	-6.69
3	0.282	0.0992	-10.56	0.6155	-4.72	45.44	-6.11
4	0.334	0.0930	-9.47	0.6011	-4.43	51.66	-5.38
5	0.383	0.0867	-8.76	0.5866	-3.84	56.59	-5.05
6	0.432	0.0796	-7.96	0.5662	-3.38	60.75	-4.93
7	0.486	0.0711	-7.15	0.5393	-2.48	64.10	-4.90
8	0.527	0.0639	-7.68	0.5154	-2.02	65.33	-5.86
9	0.573	0.0556	-8.41	0.4851	-1.40	65.66	-7.25
10	0.628	0.0451	-8.44	0.4441	0.03	63.83	-8.42
11	0.659	0.0389	-8.58	0.4194	0.59	61.19	-9.22
12	0.717	0.0269	-7.39	0.3687	3.85	52.23	-10.87
13	0.773	0.0156	8.96	0.3177	12.25	37.92	-3.03
14	0.799	0.0090	15.01	0.2909	15.42	24.64	-0.23

Model – 4 grooved design underperformed in terms of thrust for  $J$  range from 0.192 to 0.717.  $K_T$  decreased compared to baseline for the aforementioned  $J$  range between -14.01% and -7.39%. From  $J$  of 0.773, the grooved design's  $K_T$  showed small improvements.  $K_P$

decreased in the range of  $-1.4\%$  to  $-7.36\%$  for  $J$  between 0.192 and 0.573 compared to baseline. From 0.628  $J$ , the  $K_P$  showed a relative increase. The aerodynamic efficiency overall showed a decrement relative to the baseline for all  $J$  cases. The variation lied between  $-0.23\%$  and  $-10.87\%$  for the range of  $J$  considered.

### 3.3.5 Model – 5

The performance and efficiency results of Model – 5 grooved design are provided in Table 10. The relative difference between the results with baseline propeller is also listed. Model – 5 grooved design displayed underperforming  $K_T$  for  $J$  between 0.192 and 0.717. The relative difference in  $K_T$  varied between  $-5.18$  and  $-13.96\%$  for the aforementioned  $J$  range. For  $J$  of 0.773 and 0.799,  $K_T$  showed a relative increase.  $K_P$  decreased for  $J$  between 0.192 and 0.628 in the range of  $-0.33\%$  to  $-7.52\%$ . From 0.659  $J$ , the  $K_P$  increased. The  $\eta$  for the grooved propeller model decreased for all  $J$  except for the highest  $J$  of 0.799. The decrement ranged between  $-2.48\%$  and  $-8.75\%$  whereas the increment was found to be  $10.71\%$ .

Table 10. – Performance and efficiency results of Model – 5

Case	Condition	$K_T$	$\Delta K_T[\%]$	$10K_P$	$\Delta K_P[\%]$	$\eta [\%]$	$\Delta\eta [\%]$
	$J$						
1	0.192	0.1081	-13.96	0.63	-7.52	32.97	-7.13
2	0.236	0.1040	-11.92	0.62	-5.88	39.40	-6.41
3	0.282	0.0995	-10.29	0.61	-4.82	45.63	-5.73
4	0.334	0.0932	-9.22	0.60	-4.49	51.83	-5.07
5	0.383	0.0868	-8.61	0.58	-4.21	56.91	-4.51
6	0.432	0.0797	-7.86	0.56	-3.60	60.95	-4.61
7	0.486	0.0709	-7.47	0.54	-2.90	64.15	-4.83
8	0.527	0.0640	-7.52	0.51	-2.49	65.76	-5.25
9	0.573	0.0559	-7.87	0.48	-1.81	66.33	-6.32
10	0.628	0.0455	-7.77	0.44	-0.33	64.53	-7.42
11	0.659	0.0394	-7.49	0.42	0.40	62.03	-7.96
12	0.717	0.0275	-5.18	0.37	3.86	53.48	-8.75
13	0.773	0.0156	9.42	0.32	12.08	38.13	-2.48
14	0.799	0.0100	27.77	0.29	15.56	27.35	10.71

### 3.3.6 Model – 6

The performance and efficiency results of Model – 6 grooved design are provided in Table 11. The relative difference between the results with baseline propeller is also listed.

Table 11. – Performance and efficiency results of Model – 6

Case	Condition	$K_T$	$\Delta K_T[\%]$	$10K_P$	$\Delta K_P[\%]$	$\eta [\%]$	$\Delta\eta [\%]$
	$J$						
1	0.192	0.1080	-14.05	0.6351	-6.74	32.66	-7.99
2	0.236	0.1039	-11.99	0.6282	-5.11	39.05	-7.25
3	0.282	0.0987	-11.00	0.6171	-4.47	45.10	-6.81
4	0.334	0.0925	-9.93	0.6027	-4.17	51.26	-6.12
5	0.383	0.0860	-9.49	0.5852	-4.06	56.27	-5.59
6	0.432	0.0790	-8.64	0.5644	-3.68	60.48	-5.34
7	0.486	0.0706	-7.85	0.5372	-2.86	63.86	-5.25

8	0.527	0.0635	-8.31	0.5131	-2.45	65.17	-6.10
9	0.573	0.0552	-9.09	0.4823	-1.97	65.56	-7.40
10	0.628	0.0444	-10.02	0.4392	-1.08	63.43	-9.00
11	0.659	0.0380	-10.72	0.4140	-0.72	60.54	-10.18
12	0.717	0.0262	-9.55	0.3650	2.83	51.52	-12.08
13	0.773	0.0147	2.93	0.3117	10.14	36.50	-6.65
14	0.799	0.0093	19.68	0.2874	14.05	25.95	5.07

Model – 6 grooved design produced underperforming  $K_T$  for  $J$  cases 1 to 12. For cases 13 and 14,  $K_T$  showed a relative increase to baseline design.

$K_P$  showed decrement for cases 1 to 11. For cases 12 to 14, the  $K_P$  increased relative to the baseline design.

The  $\eta$  of the grooved model showed decrement for all  $J$  cases except case 14. The difference was in the range between -5.25% and -12.08%. For the last case, a small increment of 5.07% was observed.

### 3.3.7 Model – 7

The performance results of Model – 7 grooved design are provided in Table 12. The relative difference between the results with baseline propeller is also listed.

Table 12. – Performance and efficiency results of Model – 7

Case	Condition	$K_T$	$\Delta K_T$ [%]	$10K_P$	$\Delta K_P$ [%]	$\eta$ [%]	$\Delta\eta$ [%]
	$J$						
1	0.192	0.1079	-14.18	0.6322	-7.17	32.76	-7.71
2	0.236	0.1039	-11.99	0.6256	-5.50	39.21	-6.86
3	0.282	0.0992	-10.55	0.6163	-4.60	45.39	-6.22
4	0.334	0.0929	-9.52	0.6016	-4.36	51.59	-5.51
5	0.383	0.0862	-9.22	0.5841	-4.25	56.55	-5.11
6	0.432	0.0791	-8.57	0.5638	-3.79	60.60	-5.17
7	0.486	0.0707	-7.71	0.5373	-2.84	63.94	-5.13
8	0.527	0.0548	-20.75	0.4800	-8.74	60.21	-13.25
9	0.573	0.0558	-8.14	0.4860	-1.22	65.75	-7.14
10	0.628	0.0451	-8.43	0.4456	0.36	63.63	-8.71
11	0.659	0.0390	-8.45	0.4209	0.94	61.06	-9.41
12	0.717	0.0268	-7.62	0.3701	4.26	51.89	-11.44
13	0.773	0.0148	3.75	0.3178	12.31	36.08	-7.72
14	0.799	0.0090	15.29	0.2915	15.66	24.65	-0.19

Model – 7 grooved design produced lower  $K_T$  compared to baseline for  $J$  between 0.192 and 0.717. The difference lies in the range between -7.62% and -20.75%.

At higher  $J$  of 0.773 and 0.799,  $K_T$  increased relatively to 3.75% and 15.29%, respectively.  $K_P$  was found to be decreased for  $J$  between 0.192 and 0.573.

A relative difference between -1.22% and -7.17% was observed in this range. From  $J$  between 0.628 and 0.799, the  $K_P$  increased. The  $\eta$  for this model was found to be reduced for all 14 cases of  $J$  considered in this study.

### 3.4 The implication of results for UAV flight operations

Model – 1, Model – 2, Model – 5, Model – 6 grooved designs had improved  $\eta$  over baseline only for one  $J$  of 0.799. Hence the  $\eta$  improvement gained from this design is very

limited for increased UAV range and endurance. Model – 3, Model – 4, Model – 7 had no  $\eta$  improvement over baseline for all  $J$ . Hence no  $\eta$  improvement could be achieved from these models to improve range and endurance of UAV.

#### 4. CONCLUSIONS

Research on grooved design implemented on a UAV propeller has been completed. A CFD investigation is conducted on propellers with different groove sizes. 7 grooved designs with different cross-sections namely,  $0.1 \times 0.1$  mm,  $0.1 \times 0.2$  mm were studied. The performance results revealed that in most of the 7 models, the thrust was reduced for most  $J$  between 0.192 and 0.717. This implied that the presence of grooves modified the flow characteristics only to detrimentally impact the thrust performance. However, the grooves improved power performance due to torque reduction. Analysis of the  $K_P$  results showed in most of the 7 models the torque reduced compared to the baseline in the low to medium  $J$  operational range. The improvement in torque, however, did not contribute to improvement in  $\eta$  in all models. The  $\eta$  is the critical parameter for operation of propellers in a UAV's real-flight.

#### REFERENCES

- [1] M. Lazzari, D. Gioia, M. Lazzari, and D. Gioia, UAV images and historical aerial-photos for geomorphological analysis and hillslope evolution of the Uggiano medievale archaeological site, *Geomatics, Nat. Hazards Risk*, vol. **8**, no. 1, pp. 104–119, 2017, doi: 10.1080/19475705.2017.1310762.
- [2] D. E. Cook, P. A. Strong, S. A. Garrett, and R. E. Marshall, A small unmanned aerial system ( UAS ) for coastal atmospheric research : preliminary results from New Zealand, *J. R. Soc. New Zeal.*, vol. **43**, no. 2, pp. 108–115, 2013, doi: 10.1080/03036758.2012.695280.
- [3] S. Coveney and K. Roberts, Lightweight UAV digital elevation models and orthoimagery for environmental applications : data accuracy evaluation and potential for river flood risk modelling, *Int. J. Remote Sens.*, vol. **38**, no. 8–10, pp. 3159–3180, 2017, doi: 10.1080/01431161.2017.1292074.
- [4] J. P. Arroyo-mora *et al.*, Implementation of a UAV – Hyperspectral Pushbroom Imager for Ecological Monitoring, *Drones*, vol. **3**, no. 12, 2019.
- [5] T. Krajník, V. Vonásek, D. Fišer, and J. Faigl, AR-Drone as a Platform for Robotic Research and Education, in *Research and Education in Robotics -EUROBOT 2011*, 2011, pp. 172–186.
- [6] S. M. A. Aftab, A. S. M. Rafie, N. A. Razak, and K. A. Ahmad, Turbulence model selection for low reynolds number flows, *PLoS One*, vol. **11**, no. 4, pp. 1–15, 2016, doi: 10.1371/journal.pone.0153755.
- [7] H. Choi, W.-P. Jeon, and J. Kim, Control of flow over a bluff body, *Annual Review of Fluid Mechanics*, vol. **40**, School of Mechanical and Aerospace Engineering, Institute of Advanced Machinery and Design, Seoul National University, Seoul 151-744, South Korea, pp. 113–139, 2008, doi: 10.1146/annurev.fluid.39.050905.110149.
- [8] M. Amitay, D. R. Smith, V. Kibens, D. E. Parekh, and A. Glezer, Aerodynamic flow control over an unconventional airfoil using synthetic jet actuators, *AIAA J.*, vol. **39**, no. 3, pp. 361–370, 2001, doi: 10.2514/2.1323.
- [9] T. C. Corke, M. L. Post, and D. M. Orlov, SDBD plasma enhanced aerodynamics: concepts, optimization and applications, *Prog. Aerosp. Sci.*, vol. **43**, no. 7–8, pp. 193–217, 2007, doi: 10.1016/j.paerosci.2007.06.001.
- [10] J. Huang, T. C. Corke, and F. O. Thomas, Plasma actuators for separation control of low-pressure turbine blades, *AIAA J.*, vol. **44**, no. 1, pp. 51–57, 2006, doi: 10.2514/1.2903.
- [11] J. P. Bons, R. Sondergaard, and R. B. Rivir, Turbine separation control using pulsed vortex generator jets, *J. Turbomach.*, vol. **123**, no. 2, pp. 198–206, 2001, doi: 10.1115/1.1350410.
- [12] B. Nishri and I. Wygnanski, Effects of periodic excitation on turbulent flow separation from a flap, *AIAA J.*, vol. **36**, no. 4, pp. 547–556, 1998, doi: 10.2514/2.428.
- [13] A. Seifert and L. G. Pack, Active flow separation control on wall-mounted hump at high Reynolds numbers, *AIAA J.*, vol. **40**, no. 7, pp. 1363–1372, 2002, doi: 10.2514/2.1796.
- [14] D. Greenblatt and I. J. Wygnanski, Control of flow separation by periodic excitation, *Prog. Aerosp. Sci.*, vol. **36**, no. 7, pp. 487–545, 2000, doi: 10.1016/S0376-0421(00)00008-7.
- [15] D. You and P. Moin, Active control of flow separation over an airfoil using synthetic jets, *J. Fluids Struct.*,

- vol. **24**, no. 8, pp. 1349–1357, 2008, doi: 10.1016/j.jfluidstructs.2008.06.017.
- [16] J. Brandt, R. Deters, G. Ananda, and M. Selig, Small-Scale Propeller Performance at Low Speeds – Online Database, 2010. <http://www.ae.illinois.edu/m-selig/props/propDB.html> (accessed May 01, 2018).
- [17] A. M. Alakashi and I. B. Basuno, Comparison between Structured and Unstructured Grid Generation on Two Dimensional Flows Based on Finite Volume Method ( FVM ), *Int. J. Mining, Metall. Mech. Eng.*, vol. **2**, no. 2, pp. 97–103, 2014.
- [18] B. Molnar, *Comparison Of Structured And Unstructured Meshes For The Computations Of An H-Type Darrieus Wind Turbine*, Otto von Guericke University Magdeburg, Germany, 2014.
- [19] M. Husaini, Z. Samad, and M. R. Arshad, Autonomous Underwater Vehicle Propeller, in *Computational Fluid Dynamics Technologies and Applications*, no. July, Intech, 2011.